THERMOFLUID CHARACTERISTICS OF ULTRAFINE BUBBLES PRODUCED USING A SONICATION METHOD

Arif Adtyas Budiman[1,2]*, Awang Noor Indra Wardana[1], Mulya Juarsa[2], Eko Sulistio Hanam[3]
[1]Department of Nuclear Engineering and Physics Engineering Faculty of Engineering Universitas Gadjah Mada (Jl. Grafika 2, Yogyakarta 55281, Indonesia)
[2]Research Centre for Nuclear Reactor Technology, Research Organization for Nuclear Energy, National Research and Innovation Agency (KST. B.J. Habibie, Setu, Tangerang Selatan 14314, Indonesia)
[3]Functional Nano Powder University Center of Excellence (FiNder U-CoE), Universitas Padjadjaran (Jalan Raya Bandung - Sumedang KM 21, Sumedang 45363, Indonesia)

**** Corresponding author:***
e-mail: arif041@brin.go.id

Submitted: 10 December 2023
Revision Received: 21 March 2024
Accepted: 13 Mayl 2024
Published: 19 August 2024

DOI :
10.17146/jstni.2024.25.2.18

Keywords: *ultrafine bubbles, zeta potential, heat specific, sonication time, production-reduction*

Abstract *Ensuring the safety of nuclear reactors involves carefully selecting the cooling fluid for advanced passive cooling systems. The density of the cooling fluid changes with the temperature as it flows. A way to alter the density of water is by creating ultrafine bubbles with small diameters. Sonication is a faster method of producing ultrafine bubbles in pure water without infusing other gases. This study aims to establish a causal relationship between the production time and temperature changes in the thermal capacity of the sample with its specific heat. In addition, a particle size analyzer through zeta potential measurement is commonly used to detect the presence of ultrafine bubbles. Variations in the production time for ultrafine bubbles through sonication are 1, 3, 5, 7, 10, and 15 minutes. The samples were analyzed both before and after being heated. Samples sonicated for 3 and 5 minutes showed 1.1% and 0.93% increases in specific heat compared to pure water. The zeta potential value decreased as the average enlarged bubble diameter increased. The 15-minute sonication sample has a higher concentration of negative charge and the lowest Cp at 3.883 kJ/kg.K, similar to the 1-minute sample with the highest zeta potential of -28.27 mV.*

INTRODUCTION

An important aspect of advanced passive cooling systems is the choice of cooling materials. The reactor vessel resilience support system is integrated with a passive cooling system for the High-Temperature Gas-cooled Reactors (HTGRs). A Reactor Cavity Cooling System (RCCS) is part of the inherent safety system that covers the vessel with water as its coolant (1,2). The goal is to prevent radioactive material hazards and maintain safety for workers, the public, and the environment through an integrated defense system that prevents contamination. Nuclear reactor installations are also provided with accident prevention and mitigation management through integrated instrumentation and control systems (3). In case of an accident, the neutron flux control system must stop the fission reaction, and the residual heat generated must be reduced quickly to maintain the system's integrity. Both active and passive cooling systems can be used to reduce the heat in the system. The active cooling system has a forced convection mechanism to transfer heat through a coolant flow generated from a pressurized pump, in contrast to the passive cooling system, whose heat transfer mechanism is based on natural circulation. Learning from the failure of the active cooling system to remove the heat of the reactor core after a power outage, the passive cooling system model is expected to maintain structural integrity without relying on pumps to generate flow (4,5). The working principle of the passive cooling system is to utilize the phenomenon of natural circulation (convection heat transfer) in the system so the flow can be formed. The mechanism occurs when there is a difference in working fluid temperature and height between the heat exchanger system and the heat source. Water is a commonly used working fluid because it has a higher specific heat than air. The absorption time of heat by water is faster but slower to release it when compared to air.

The analysis in a comparison of the ability of fluid with and without ultrafine bubbles to absorb and release heat has been carried out by Senthilkumar G. et al. It takes a longer time for a fluid with ultrafine bubbles to absorb heat than a fluid without ultrafine bubbles (6). Fluids or water that have ultrafine bubbles have lower heat absorption, but with a slight heating can generate natural circulation flow. Ultrafine bubbles are air or gas bubbles measuring less than 1 µm in diameter that are dispersed into the water medium (7,8). One of the characteristics of small bubble diameter size is the negative zeta potential value in millivolts (mV). The zeta potential of the working fluid can be altered by

external treatment of ultrafine bubbles. Increasing zeta potential value indicates the expansion of the diameter of ultrafine bubbles. Besides stability, ultrafine bubble diameter size distribution uniformity is also important for the cooling function. This parameter supports effective heat absorption if ultrafine bubbles at sizes up to 50 nm do not enlarge during heating above 40 ℃ (9). Particle Size Analyzer (PSA) determines the average hydrodynamic diameter of particles using the polydispersity index (PI). This measurement method has a limited condition that requires the fluid temperature when measured to be conditioned at room temperature (25 ℃). This is due to the nature of ultrafine bubbles that have Brownian motion to provide a measurable state. Ultrafine bubbles in water have charged layers that surround the gas phase. They are highly pressurized and can be affected by temperature and shock, causing changes in the charge and bubble size (10). Researchers have used several production methods to study the characteristics of ultrafine bubbles in solution. Table 1 shows the previous research that was carried out using mechanical production methods (stirring) and sonication.

In Table 1, this study has mainly discussed two sections, i.e. the thermal and zeta potential characterization of ultrafine bubbles produced by sonication. Considering the change of mass samples is proportional to their specific heat, the thermal management of samples before and after heating should be investigated. The production of ultrafine bubbles is conducted at a working frequency of 40 kHz with sonication times of 1, 3, 5, 7, 10, and 15 minutes and temperature variations are conducted up to 70 ℃.

Table 1. Ultrafine bubbles research status

Research Objectives	**K. Yasuda et al. (2018)**	**G. Senthilkumar et al. (2020)**	**S. Tanaka et al. (2021)**	**Mingbo Li et al. (2021)**	**Present (2023)**
Temperature	24 ℃ – 25 ℃	40 ℃ – 90 ℃	25 ℃ – 26 ℃	10 ℃ – 70 ℃	25 ℃ – 80 ℃
Production time	5, 10, 15, 20, 25, and 30 min (f = 22kHz, 43kHz, 129 kHz, 488 kHz, and 1MHz)			5 – 35 min	1, 3, 5, 7, 10, and 15 min (f = 40kHz)
Reduction time	(same as production time)		5, 15, and 30 min (f = 1,6MHz)		
Production method	Bath-type sonication	Mechanical stirring	Pressure differential and mechanical stirring	Immersion probe (horn) type sonication	Bath-type sonication
Reduction method			Bath-type sonication		
Electrical Conductivity			✓		✓
pH			✓		
DO			✓		
Zeta potential			✓	✓	✓
Diameter size	✓			✓	
Thermal conductivity		✓			
Viscosity		✓			
Surface tension		✓			
Specific Heat					✓

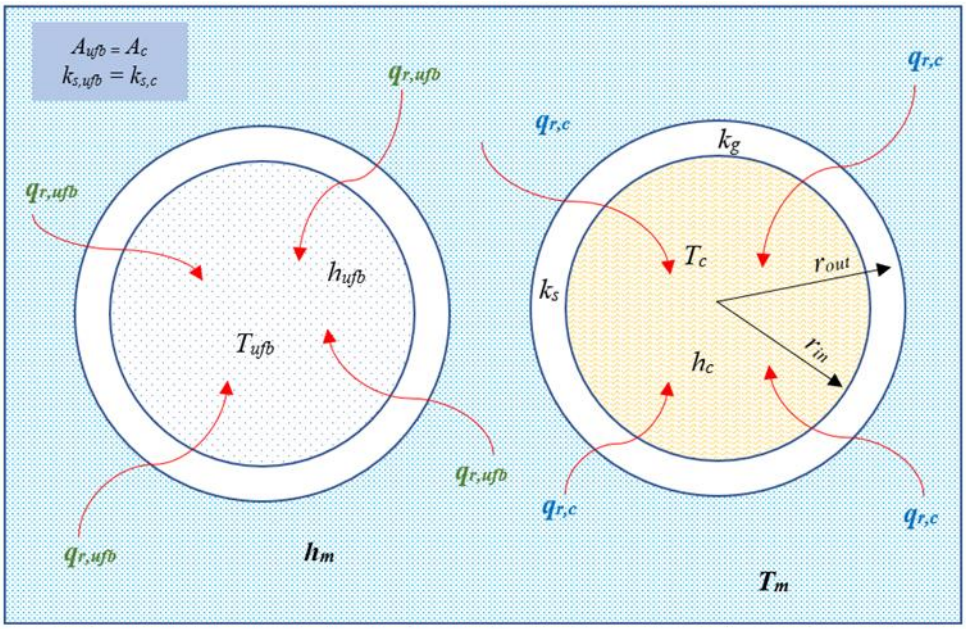

Figure 1. Schematic of the steady-state approach of mixed heat transfer (top view).

Unlike the previous studies, the ultrafine bubbles that are produced by sonication have a tighter production–reduction region and heat accumulation. In addition, due to the lack of a cooling system for maintaining the quality of samples, the maximum production time is stated as 15 minutes. The working frequency of ultrasonic transducers is maintained at 40kHz. This research objective is to get a causal relationship between ultrafine bubble thermal capability by varying production time and thermal treatment. The thermal capability analysis will focus on specific heat based on the mass samples measurement.

EXPERIMENTAL SECTION

Ultrafine Bubbles Production: Sonication Method

One of the methods to produce ultrafine bubbles is sonication. Sonication is the process of delivering ultrasonic waves to a target material for modification purposes. Ultrafine bubbles can be produced by sonication using two models: a horn-type probe inserted into water and a bath-type probe attached to a wall or container. Sonication involves the formation or alteration of bubble nuclei through collisions between bubbles in a stationary wave region. Longer sonication time forms larger ultrafine bubbles, some rupturing and transforming into the production-reduction cycle (8).

Zeta Potential

In general, the mixture between two heterogeneous substances that experience the Tyndall effect has an ionic charge known as zeta potential. The magnitude of the zeta potential indicates the potential stability of the colloidal system. The size of the bubble diameter is proportional to its zeta potential in volumetric measurements. The bubble size increases as the zeta potential becomes more positive. Thus, if the zeta potential is more negative, then it tends to shrink the bubble size and make it able to remain in the dispersant medium. The magnitude of zeta potential can change when the temperature changes (11). In a heterogeneous sample of ultrafine bubbles, the temperature increase leads to the microbubble size enlarging faster than the bubble size below 50 nm. This allows the zeta potential of the sample to increase after heating (9).

Heat Transfer and Specific Heat of Ultrafine Bubbles

The energy passed through the medium will be absorbed and transmitted. The first law of thermodynamics states that energy is conserved within a system. Energy transfer resulting in temperature change occurs through conduction, convection, and radiation. Figure 1 describes the apparatus scheme of the sample in a steady state.

Based on Figure 1, when the total heat transfer of the control sample is the same as the ultrafine bubbles sample ($q_{r,c} = q_{r,ufb}$), then it can be stated as;

$$q_{r,c} = \frac{T_m - T_c}{R_{w,total}} \text{ and } q_{r,ufb} = \frac{T_m - T_{ufb}}{R_{ufb,total}} \quad (1)$$

then multi-layer heat transfer involves conduction-convection with resistance or thermal resistance (R) fulfilled by;

$$R_{ufb,total} = \frac{1}{2\pi L r_{in} h_{ufb}} + \frac{ln\left(\frac{r_{out}}{r_{in}}\right)}{2\pi L k_s} + \frac{1}{2\pi L r_{out} h_m}$$

and

$$R_{w,total} = \frac{1}{2\pi L r_{in} h_c} + \frac{ln\left(\frac{r_{out}}{r_{in}}\right)}{2\pi L k_s} + \frac{1}{2\pi L r_{out} h_m} \quad (2)$$

where ***L*** (m) is the height of the submerged sample and k_s is the thermal conductivity of glass, which is 0.8 W/m.K (12). Table 2 presents the range of ***h*** values in the medium of water and air under various heat transfer conditions. With ***h*** (W/m^2.K) is the fluid's ability to receive and transmit heat, known as the convection heat transfer coefficient.

Table 2. Convection heat transfer coefficient of water and air

Heat transfer conditions, *h*	**W/m^2.K**
Gas or air, natural convection	5 – 37 (13) 2,5 – 25 (14)
Air, forced convection	10 – 500 (14)
Water, natural convection	100 – 1200 (13)
Water, forced convection	100 – 15000 (14)
Water, nucleate boiling	2000 – 45000 (13)
Water, boiling	2500 – 25000 (14)
Water, film boiling	100 – 300 (13)

Ultrafine bubbles fluid is a mixture of water and air or dissolved gas. The specific heat of ultrafine bubbles can be obtained through mass measurement. The relationship of heat energy absorption in a fluid with a certain mass at a certain temperature has the following general form;

$$Q = m.Cp.dT \quad (3)$$

Specific heat (***Cp***) is one of the thermal properties of a fluid, defined as the amount of heat required to increase the temperature of a fluid of mass (***m***) 1 kg by 1 ℃. The amount of specific heat of pure water (***w***) and ultrafine bubbles (***ufb***) can be calculated with a limitation approach under the condition that the energy absorbed by both is the same, so $Q_w = Q_{ufb}$. If, $\rho = \frac{m}{V}$ with the volume of pure water and ultrafine bubbles are the same, then;

$$Cp_{ufb} = \frac{\rho_w.Cp_w(T_x - T_0)_w}{\rho_{ufb}(T_x - T_0)_{ufb}} \quad (4)$$

Where T_x is expressed as the measurement of the targeted temperature and T_0 is the initial temperature. If $(T_x - T_0)_w = (T_x - T_0)_{ufb}$, then the specific heat of ultrafine bubbles fluid is obtained from;

$$Cp_{ufb} = \frac{\rho_w.Cp_w}{\rho_{ufb}} \quad (5)$$

The specific heat of water at 25℃ and 70℃ is 4.182 kJ/kg.K (15) and 4.190 kJ/kg.K (15,16), respectively. Water density ***ρ*** (kg/m^3) decreases with temperature, but air density decreases with increasing temperature.

Data Acquisition System

The data acquisition system includes hardware and software for signal conditioning and communication with a PC. The condition module comprises a series of analog signal conditioners that are executed via control commands, according to the program. LabVIEW is a software system used to create virtual diagrams, display measurement results, and execute data-based commands. The LabVIEW-based data acquisition system is widely used in laboratories due to its high accuracy and design flexibility (17). The NI 9214 device is commonly used as a temperature recorder because it allows for easier data analysis (18,19). NI cDAQ 9188 serves as the chassis for the communication module with the PC (20).

Methods

In preparation, the transducer was protected from overheating by filling the sonicator with pure water in a bath-type setup. To ensure optimal performance of the ultrasonic transducers, kindly conduct a power measurement for 1 minute. K-type thermocouples are tested between 30 ℃ to 95 ℃ with a standard deviation of less than 0.3. The experiment involves producing ultrafine bubbles by sonication of 350 mL pure water in BAKU BK-2000 for several durations: 1, 3, 5, 7, 10, and 15 minutes. Zeta potential measurements are taken at 25 ℃ using a Malvern Zetasizer Nano ZS. A total of 200 mL is heated to 90 ℃, while 50 mL is used as a sample for zeta potential measurement. The first experiment aims to get the thermal capability of ultrafine bubbles. Water samples are sonicated at different durations, starting below 25 ℃ and reaching 80 ℃.

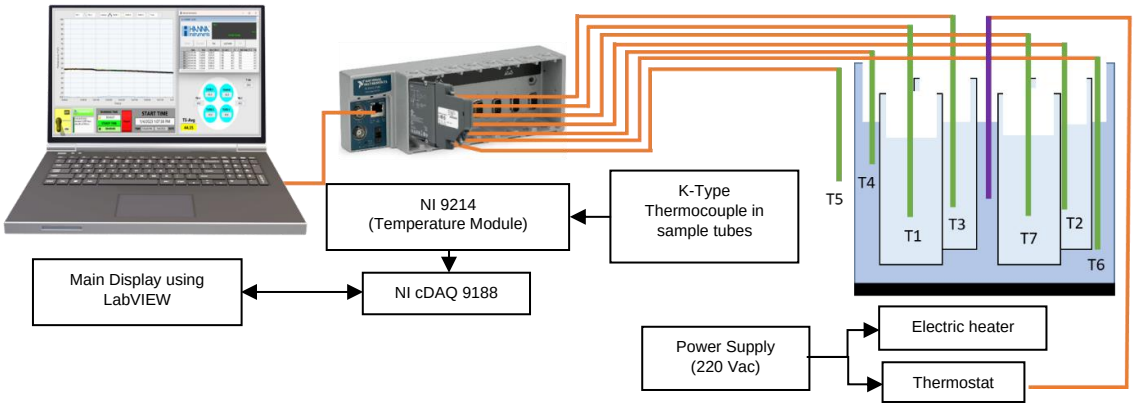

Figure 2. Schematic of the apparatus system.

The specific heat of ultrafine bubbles is obtained using the temperature change relationship between samples under steady-state according to equation no. 5. The transparent vessel sample uses glass materials. It is placed in a big transparent glass vessel with a reference (pure water). Figure 2 describes the thermal testing scheme of the sample under steady state. The heat energy absorbed through the glass container is calculated through;

$$q_{conduction} = \frac{T_{heater} - T_m}{R_m}$$

And

$$q_{conduction} = \frac{T_{heater} - T_m}{\frac{ln\left(\frac{r_{out}}{r_{in}}\right)}{2\pi L k_g}} \quad (6)$$

k_g is the thermal conductivity of borosilicate glass, which is 1.10 W/m.K (21), while L is the height of the water pool, which is 10 cm. The heat energy released by the heater of 500 W is operated until the water pool temperature reaches 80 °C. The pool water convection heat transfer coefficient (h_m) at a steady state at 80 °C is obtained through correlation;

$$h_m = \frac{q_{conduction}}{A_m(T_{heater} - T_m)} \quad (7)$$

To obtain the convection heat transfer coefficient of the reference sample (h_c), a steady state is maintained at that temperature. The value of h_c can be calculated using the Rayleigh number from (22,23) that satisfies;

$$Ra_D = \frac{g\beta(T_m - T_c)D^3}{\nu\alpha} \quad (8)$$

where T_m and T_c are the bulk temperatures of the pool water and reference sample, respectively. While the acceleration of gravity g (m/s^2), thermal expansion β (1/K), and cylinder inner diameter D (m) are inversely proportional to kinematic viscosity ν (m^2/s) and thermal diffusivity α (m^2/s). The thermal diffusivity of the reference sample is obtained through the relationship of thermal conductivity k (W/m.K) to density ρ (kg/m^3) and specific heat Cp (kJ/kg.K) which fulfills the equation;

$$\alpha = \frac{k}{\rho C_p} \quad (9)$$

Based on **RaD**, the Nusselt number for the reference sample in cylindrical geometry is obtained by;

$$Nu_D = \frac{hD}{k} = CRa_D{}^n \quad (10)$$

The constants **C** and **n** are known based on Table 3. Thus, the value of h_c obtained from equation (10) becomes;

$$h = \frac{Nu_D k}{D} \quad (11)$$

Table 3. Values of C and n on RaD (23)

RaD	C	n
1 x 10^{-10} to 1 x 10^{-2}	0.675	0.058
1 x 10^{-2} to 1 x 10^{2}	1.02	0.148
1 x 10^{2} to 1 x 10^{4}	0.850	0.188
1 x 10^{4} to 1 x 10^{7}	0.48	0.25
1 x 10^{7} to 1 x 10^{12}	0.125	0.333

Furthermore, after h_m, h_c, and the value of the convection transfer coefficient of ultrafine bubbles are obtained, the value of h_{ufb} is fulfilled;

$$h_{ufb} = \frac{\alpha}{(1-\alpha)\left(\frac{ln\left(\frac{r_{out}}{r_{in}}\right)}{2\pi L k_s} + \frac{r_{in}}{r_{out} h_m}\right) + \frac{1}{h_c}} \quad (12)$$

If, $(1-\alpha) = 1 - \frac{T_m - T_c}{T_m - T_{ufb}} = \left(\frac{T_m - T_{ufb}}{T_m - T_{ufb}}\right) - \left(\frac{T_m - T_c}{T_m - T_{ufb}}\right) = \frac{T_c - T_{ufb}}{T_m - T_{ufb}}$, then, after $1-\alpha$ is substituted into equation (12), the convection heat transfer coefficient of ultrafine bubbles, h_{ufb} can be identified through;

$$h_{ufb} = \frac{T_m - T_c}{T_c - T_{ufb}\left(\frac{r_{in} ln\left(\frac{r_{out}}{r_{in}}\right)}{k_s} + \frac{\left(\frac{r_{in}}{r_{out}}\right)}{h_m}\right) + \frac{(T_m - T_c)}{h_c}} \quad (13)$$

RESULTS AND DISCUSSION

Convective Heat Transfer (*h*) and Specific Heat at Constant Pressure (*Cp*) Profiles

The maximum ultrafine bubble production time is limited to 15 minutes, as the temperature effects of sonication are significant. After the samples are produced and heated under atmospheric conditions, they are then cooled under room conditions sustained at 20.41 °C to 21.13 °C. The experiment is conducted for 4.16 hours with the boundary temperature set at 80 °C. The sample thermal testing model is conducted in a glass vessel containing one reference and three test samples for one test. The first includes the reference sample, 1, 10, and 15-minute samples. Then followed by the reference sample (zero), 3, 5, and 7 minutes. The heated process of the samples is carried out until it reaches the target temperature ($T_{setting}$) at 80 °C. The heat transfer profile that occurred in each sample is plotted in the curve in Figure 3. The convection heat transfer involves the combined effects of energy transfer from conduction and fluid movement (24). The dashed horizontal line along the x-axis represents the convection heat transfer coefficient of the 0-min sample, which is 313.94 W/m^2.K. Based on the calculations, the obtained heat transfer coefficient results are within the range corresponding to Table 2, i.e., natural convection. According to Figure 3, samples 1, 7, 10, and 15 min show a positive temperature difference in the 0-min sample. A notable finding is the change in convection heat transfer coefficient, which tends to be greater during the heating process at 3 and 5-min samples. The ***h***-value gap between the 0-min sample and the 3-min sample is 90.59 W/m^2.K.

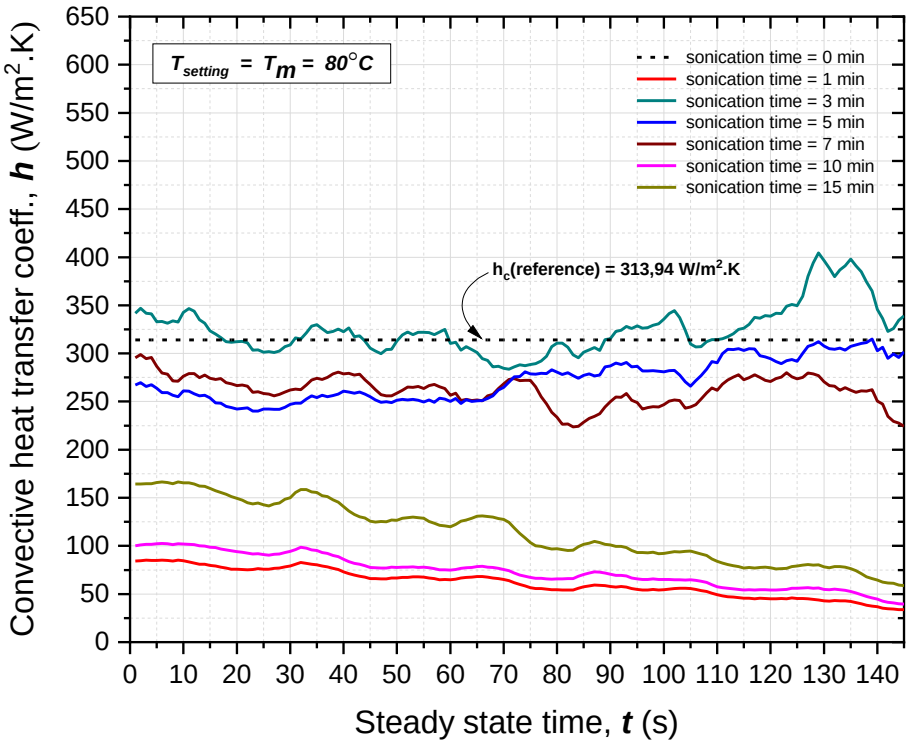

Figure 3. The convection heat transfer profile of ultrafine bubbles fluid.

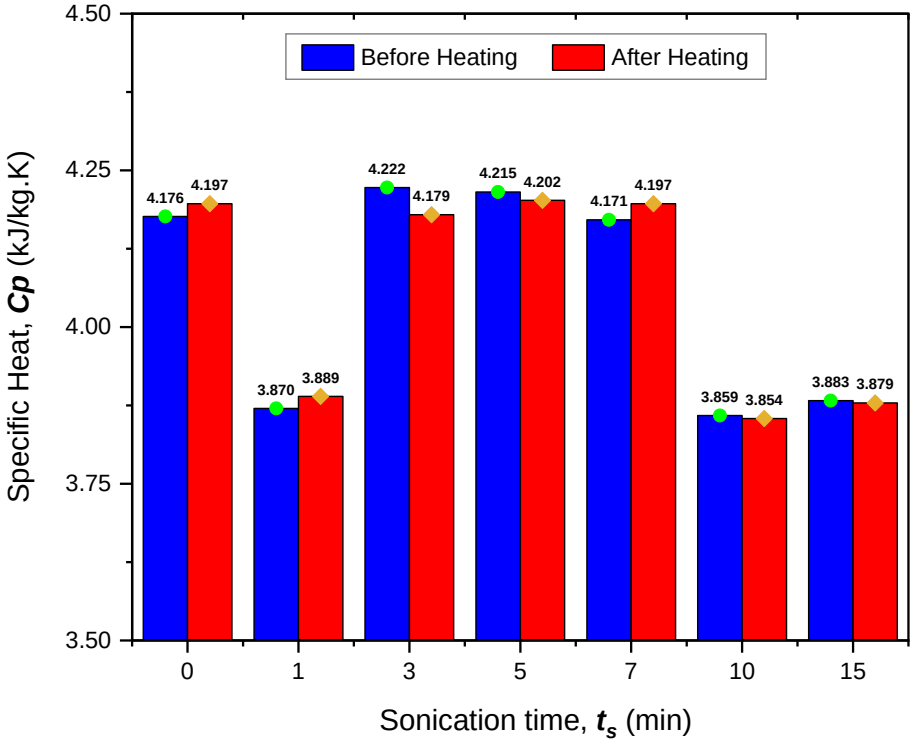

Figure 4. The specific heat profile of ultrafine bubbles fluid.

The natural cooling procedure is carried out after heating the samples so that the mass and zeta potential are measured at the same temperature. Mass measurements are performed three times to determine the amount of measurement deviation. The sample with 5 min sonication time has the highest standard deviation, which is 2.94732 x 10^{-6}. Based on the average mass measurement, then calculated using equation no. 5 to obtain the amount of heat capacity. The specific heat is calculated using equation 5 once the steady state is achieved at 80 ℃. The calculation of the specific heat of the sample is carried out before and after heating, i.e., at 25 °C and 80 °C. Based on the calculation results, the specific heat profile of ultrafine bubbles is plotted in Figure 4. It shows that $Cp_{reference}$ before heating is 4.176 kJ/K and increased after heating to 4.197 kJ/kg.K. Based on Figure 4, the increased density after heating is the 0, 1, and 7-minute samples, while the other samples decreased by different values.

The specific heat for the 1-minute sample, Cp_1 is 3.870 kJ/kg.K then increased to 3.889 kJ/kg.K and Cp_7 are 4.171 to 4.197 kJ/kg.K after heating. Meanwhile, Cp_3 of 4.222 kJ/kg.K decreased to 4.179 kJ/kg.K after heating. Similarly to Cp_3, Cp_5 also decreased from 4.215 kJ/kg.K to 4.202 kJ/kg.K. As well as the Cp_{10}, which has an initial specific heat (before heating) of 3.859 kJ/kg.K, then decreased to 3.854 kJ/kg.K. In addition, for the sample of 15 minutes, the specific heat decreased from 3.883 to 3.879 kJ/kg.K.

The relationship of specific heat to sonication time and temperature change showed significance with a maximum p-value of 0.021 (statistically significant). Furthermore, the thermal characteristics of the ultrafine bubbles and the reference fluid are studied via zeta potential measurements.

Zeta potential analysis

Zeta potential measurements are conducted before and after heating. The period between the end of the heating process and the measurement is around 96 hours. The interpretation of zeta potential difference (dZP) in this study indicates that if it shifts in a positive direction, then it has a negative indication, and vice versa. This will help to analyze the trend of bubble diameter change and the tendency of survival time. The relationships between the differences in specific heating, zeta potential, and total counts with indications of possible phenomena are shown in Table 4.

Table 4. Characterization of the ultrafine bubbles production using the sonication method

Condition*	Sample [min]	dCp_{r-s} [kJ/kg.K]	dZP_T [mV]	dki_T [*count*]	dZP_{r-s} [mV]	dki_{s-r} [*count*]	Sample Indication
BH	0	0	1,46	21200	0	0	Reference
AH	(ref)	0			0	0	*t-T*$_{maks}$ = reduction; $\underline{D}_{ufb}$ >>; $t_{disperse}$ <<;
BH	1	0.3063	12,97	-10380	-6,17	-31400	*t-T*$_{min}$ = reduction; $\underline{D}_{ufb,1}$ >>; $t_{disperse,1}$ <<;
AH		0.3074			8,26	-20580	*t-T*$_{maks}$ = **production**; $\underline{D}_{ufb,1h}$ <<; $t_{disperse,1h}$ <<;
BH	3	-0.0460	4,14	-38470	-7,02	-6000	*t-T*$_{min}$ = reduction; $\underline{D}_{ufb,3}$ >>; $t_{disperse,3}$ <<;
AH		0.0175			-1,42	-23270	*t-T*$_{maks}$ = reduction; $\underline{D}_{ufb,3h}$ >>; $t_{disperse,3h}$ <<;
BH	5	-0.0390	0,64	1063250	-5,43	-83250	*t-T*$_{min}$ = reduction; $\underline{D}_{ufb,5}$ >>; $t_{disperse,5}$ >>;
AH		-0.0052			-3,33	1001200	*t-T*$_{maks}$ = reduction; $\underline{D}_{ufb,5h}$ >>; $t_{disperse,5h}$ <<;
BH	7	0.0055	0,56	51260	-6	-57360	*t-T*$_{min}$ = reduction; $\underline{D}_{ufb,7}$ >>; $t_{disperse,7}$ >>;
AH		0.0001			-3,98	15100	*t-T*$_{maks}$ = reduction; $\underline{D}_{ufb,7h}$ >>; $t_{disperse,7h}$<<;
BH	10	0.3176	-8,06	175850	-39,77	381450	*t-T*$_{min}$ = reduction; $\underline{D}_{ufb,10}$ >>; $t_{disperse10}$ <<;
AH		0.3428			-30,25	578500	*t-T*$_{maks}$ = reduction; $\underline{D}_{ufb,10h}$ >>; $t_{disperse,10h}$ <<;
BH	15	0.2937	14,55	92800	-11,15	25100	*t-T*$_{min}$ = reduction; $\underline{D}_{ufb,15}$ >>; $t_{disperse,15}$ <<;
AH		0.3179			4,86	139100	*t-T*$_{maks}$ = **production**; $\underline{D}_{ufb,15h}$<<; $t_{disperse,15h}$<<;

Note : *sample condition AH (*after heating*) and BH (*before heating*)

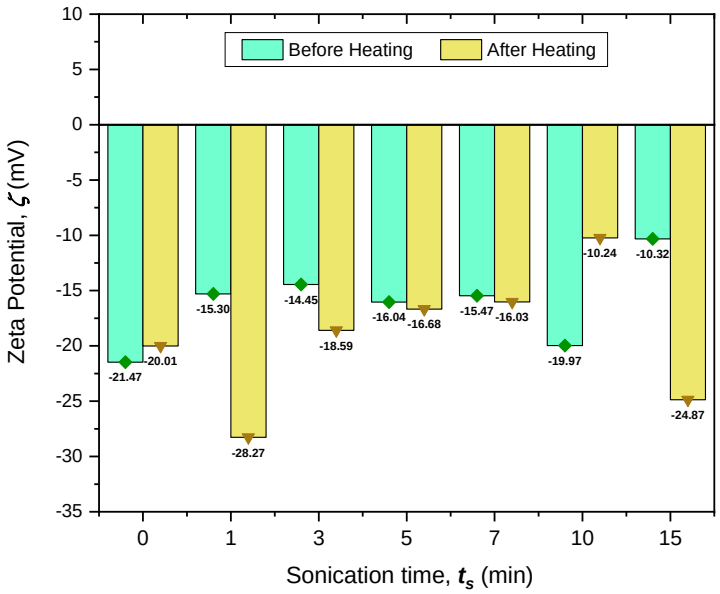

Figure 5. Zeta potential profile of the sample.

Based on Table 6, *t-T$_{min}$* means the sample before heating and *t-T$_{max}$* means the sample after heating. $\underline{\boldsymbol{D}}_{\boldsymbol{ufb}}$ denotes the average diameter of ultrafine bubbles in the pre-heated condition. Meanwhile, the additional subscript notation ***h*** becomes $\underline{\boldsymbol{D}}_{\boldsymbol{ufb,h}}$ denotes after heating. As indicated in Table 6, (*dki$_{s-r}$*) and (*dZP$_{r-s}$*) before heating are both positive, meaning that the sample could potentially have a longer time duration (*t$_{disperse}$*) in water with a smaller average diameter ($\underline{D}_{ufb}$). The negative sign of the sample's specific heat difference against the 0-min sample (*dCp$_{r-s}$*) may be interpreted as the ultrafine bubble's thermal ability to absorb and release more heat compared to the 0-min sample. The optimal production of ultrafine bubbles occurred after the sample with a sonication time of 15 min was heated at *T$_{setting}$* = 80 ℃.

The zeta potential profiles of the samples are shown in Figure 5. The zeta potential of the 1-min sample compared to the 0-min sample before heating shows a significant difference. In other words, the zeta potential shifted in a positive direction towards the reference (*dZP$_{1,r-s}$* = -6.17 mV). Then, it shifts to a negative direction after heating, which is *dZP$_{1,T}$* = 8.26 mV. For the 0-min sample, the changes in zeta potential values before and after heating is *dZP$_{0,T}$* = -1.46 mV. The total count represents the number of instances of light beams detected as bubble concentration. The difference between the total counts of the 1-min sample and 0-min (*dki$_{1,s-r}$*) in the pre- and post-heated conditions are -31400 and -20580, respectively. In this case, the sample has a much more negative zeta potential than the 0-min sample after heating. It seems possible that ultrafine bubbles with a certain diameter size can withstand temperature changes (9). At the same time, increased temperature has the potential to produce fine bubbles besides enlarging and rupturing microbubbles. The zeta potential after 3 minutes of ultrafine bubbles production moves in a positive direction towards the 0-min sample. After being heated, the zeta potential increased (moving in the negative direction) to -18.59 mV from -14.45 mV. Before heating, the zeta potential difference with the 0-min sample (*dZP$_{3,r-s}$*) is -7.02 mV; meanwhile, it is decreased (*dZP$_{3,T}$*) by -1.42 mV after heating.

The total counts difference 3-min sample against the 0-min sample (*dki$_{3,s-r}$*) in the pre- and post-heated conditions are -6000 and -23270, respectively. In Figure 5, samples that decreased in zeta potential (more positive) after production indicate that the regime formed is the reduction regime. Meanwhile, the dominant production regime is indicated after the sample is heated.

The zeta potential difference between the 0-min sample and the 5-min sample (*dZP$_{5,r-s}$*) under pre- and post-heating conditions are -5.43 mV and -3.33 mV, respectively. Meanwhile, the total count differences of the sample against the reference (*dki$_{5,s-r}$*) in the pre-and post-heated conditions are -83250 and 1001200, respectively. After heating, a 5-minute sample zeta potential is shifted to more negative with a difference (*dZP$_{5,T}$*) of 0.64 mV. Interestingly, its total count has a difference (*dki$_{5,T}$*) of 22 times the total count before heating, which reached 1063250. In the other samples, the change in total counts after heating is not as high as this. A greater difference in concentration or total count (positive value) allows the ultrafine bubbles existing in the sample to stay longer.

Based on Table 6, the zeta potential change of the 7-min sample shows different behaviour from 1 and 3-min samples but is similar to the 5-min sample under pre- and post-heating conditions. The zeta potential difference of the 7-min sample after heating (*dZP$_{7,T}$*) is 0.56 mV. Meanwhile, its zeta potential difference against the 0-min sample (*dZP$_{7,r-s}$*) before and after heating is -6 mV and -3.98 mV, respectively. At the same time, the difference between its total count and the 0-min sample count (*dki$_{7,s-r}$*) under these conditions are -57360 and 15100, respectively. In comparison, the difference in total counts due to heating (*dki$_{7,T}$*) is 51260. Shifting the zeta potential to the positive direction has the potential to increase the size of the bubble diameter (undergoing a reduction process). However, after thermal testing, the 7-minute sample was able to narrow the difference to -3.98mV against the reference, which means that during the heating process, ultrafine bubbles were also produced.

In Table 6, the difference between the charge concentration of the sample and the reference (*dki$_{10,s-r}$*) before heating is 381450. After heating, the difference between the 10-min and 0-min samples reached 578500. Meanwhile, its zeta potential difference (*dZP$_{10,r-s}$*) before and after heating are - 39.77 mV and -30.25 mV, respectively. Meanwhile, the zeta potential difference due to heating (*dZP$_{10,T}$*) is -8.06 mV. Similar to the sample with a sonication time of 7 minutes, the reduction of ultrafine bubbles is identified. The charge concentration (total counts) increases in the 5-min and 7-min samples, compared to the 0-min sample. In terms of the

specific heat difference (dCp_{r-s}) against the reference, a positive value indicates that the sample has a reduction regime. Still, with a high total count, the dispersed ultrafine bubbles have a greater number.

The difference between the total number of samples and the reference ($dki_{15,s-r}$) is 139100 with a difference ($dZP_{15,r-s}$) of 4.86 mV, which means that the zeta potential value is increasingly negative, as shown in Figure 5. Before heating, the reference had a difference of -11.15 mV compared to the sample, indicating a reduction regime in the sonication. The zeta potential values for the sample sonicated for 15 minutes are similar to those for the sample sonicated for 1 minute. The 15-min sample zeta potential decreased ($dZP_{15,T}$) by 14.55 mV, while the 0-min sample only decreased ($dZP_{r,T}$) by -1.46 mV after heating. Negative zeta potential and positive charge concentration indicate changes in ultrafine bubble size and longevity in water (11).

CONCLUSION

A production method to produce ultrafine bubbles using sonication has been conducted and characterized. The variation of production time and heat treatment is carried out to obtain the production characteristics. The thermal characteristics of ultrafine bubbles were analyzed using specific heat. The Cp of the 15-minute sample was the lowest at 3.883 kJ/kg.K. However, after heating, it exhibited a higher and more negative zeta potential charge concentration, similar to the 1-minute sample. Samples with sonication times of 5, 7, 10, and 15 minutes have large charge concentrations or are identical to the length of time ultra-fine bubbles can sustain in water. The sonication method has production and reduction regimes. The longer production time cannot ensure that the zeta potential concentration increases unless the optimal time limit is known through production characterization. When a fluid containing ultrafine bubbles is heated, air bubbles emerge through the container's pores, which increases the concentration of H^+ ions and produces a more negative zeta potential. This research is an initial study that notes further characterization activities. Some characterization can be done through observation of the fluid flow of ultrafine bubbles in a closed loop with a natural circulation flow generation mechanism to investigate the velocity profile.

ACKNOWLEDGEMENTS

This research was funded by the "Riset Inovasi untuk Indonesia Maju" (RIIM) batch 1 grant for 2022-2025 with contract number B-811/II.7.5/FR/6/200 and B-2103/III.2/HK.04.03/7/2022. Thank you to the Research Centre for Nuclear Reactor Technology head, Research Organization for Nuclear Energy (BATAN), and National Research and Innovation Agency (BRIN). Also, special thanks to all members of Nuclear Reactor Thermal-Fluids System Development (NRTFSyDev) and support by FiNder U-CoE Padjadjaran University. The authors acknowledge the facilities, scientific and technical support from the Nuclear Advanced Materials Laboratory, National Research and Innovation Agency through "*E- Layanan Sains-BRIN"*. Arif Adtyas Budiman, Awang Noor Indra Wardana, and Mulya Juarsa are the main contributors. All authors read and approved the final version of the article.

REFERENCES

1. Kusumastuti R, Sriyono, Juarsa M, Tjahjono H, Irianto ID, Setiadipura T, et al. Reactor Cavity Cooling System with Passive Safety Features on RDE: Thermal Analysis During Accident. Tri Dasa Mega [Internet]. 2019;21(2):87–93. Available from: http://dx.doi.org/10.17146/tdm.2019.21.2.5499
2. Kwiatkowski T, Jędrzejczyk M, Shams A. Numerical Study of The Flow and Heat Transfer Characteristics in a Scale Model of The Vessel Cooling System for The HTTR. Nuclear Engineering and Technology [Internet]. 2023;(October). Available from: https://doi.org/10.1016/j.net.2023.11.035
3. Björkman K, Pakonen A. Analyzing Defense-in-Depth Properties of Nuclear Power Plant Instrumentation and Control System Architectures Using Ontologies. Proceedings of 13th Nuclear Plant Instrumentation, Control and Human-Machine Interface Technologies, NPIC and HMIT 2023 [Internet]. 2023;1590–9. Available from: https://doi.org/10.13182/NPICHMIT23-41042
4. Zhang W, Hao W, Ye Z, Xie H, Shi L. Conceptual Design and Analysis of a Combined Passive Cooling System for Both Reactor and Spent Fuel of The Pool-Vessel Reactor System. Nuclear Engineering and Design [Internet]. 2023;414(May):112557. Available from:

https://doi.org/10.1016/j.nucengdes.2023.112557

5. Surip W, Putra N, Antariksawan AR. Design of Passive Residual Heat Removal Systems and Application of Two-Phase Thermosyphons: A review. Progress in Nuclear Energy [Internet]. 2022;154(October):104473. Available from: https://doi.org/10.1016/j.pnucene.2022.104473
6. Senthilkumar G, Rameshkumar C, Nikhil MNVS, Kumar JNR. An Investigation of Nanobubbles in Aqueous Solutions for Various Applications. Applied Nanoscience (Switzerland) [Internet]. 2018;8(6):1557–67. Available from: http://dx.doi.org/10.1007/s13204-018-0831-8
7. Tanaka S, Kobayashi H, Ohuchi S, Terasaka K, Fujioka S. Destabilization of Ultrafine Bubbles in Water Using Indirect Ultrasonic Irradiation. Ultrasonics Sonochemistry [Internet]. 2021;71:105366. Available from: https://doi.org/10.1016/j.ultsonch.2020.105366
8. Yasuda K, Matsushima H, Asakura Y. Generation and Reduction of Bulk Nanobubbles by Ultrasonic Irradiation. Chemical Engineering Science [Internet]. 2019;195:455–61. Available from: https://doi.org/10.1016/j.ces.2018.09.044
9. Li M, Ma X, Eisener J, Pfeiffer P, Ohl CD, Sun C. How Bulk Nanobubbles are Stable Over a Wide Range of Temperatures. Journal of Colloid and Interface Science [Internet]. 2021;596:184–98. Available from: https://doi.org/10.1016/j.jcis.2021.03.064
10. Tanaka S, Terasaka K, Fujioka S. Generation and Long-Term Stability of Ultrafine Bubbles in Water. Chemie-Ingenieur-Technik [Internet]. 2021;93(1–2):168–79. Available from: https://doi.org/10.1002/cite.202000143
11. Meegoda JN, Aluthgun Hewage S, Batagoda JH. Stability of Nanobubbles. Environmental Engineering Science [Internet]. 2018;35(11):1216–27. Available from: https://www.liebertpub.com/doi/10.1089/ees.2018.0203
12. Venkataramanaiah P, Aradhya R, Rajan J S. Investigations on The Effect of Hybrid Carbon Fillers on The Thermal Conductivity of Glass Epoxy Composites. Polymer Composites [Internet]. 2021;42(2):618–33. Available from: http://dx.doi.org/10.1002/pc.25852
13. Kuganov VA. Heat Transfer Coefficient [Internet]. [cited 2023 Feb 8]. Available from: https://dx.doi.org/10.1615/AtoZ.h.heat_transfer_coefficient
14. Kosky P, Balmer R, Keat W, George Wise. Chapter 12 - Mechanical Engineering. In: Hayton J, editor. Exploring Engineering (Third Edition) [Internet]. 3rd ed. London: Elsevier; 2013. p. 264. Available from: https://doi.org/10.1016/B978-0-12-415891-7.00012-1
15. Long J, Jiang H, Liao C, Hu Q, Zhang Y, Zhang R. Heat Load-Carrying Capacity of Surface Water Source Combined With Stagnant Water and River Water. Renewable Energy [Internet]. 2023;207(April 2022):286–97. Available from: https://doi.org/10.1016/j.renene.2023.03.046
16. Wonorahardjo S, Sutjahja IM, Kurnia D. Potential of Coconut Oil for Temperature Regulation in Tropical Houses. Journal of Engineering Physics and Thermophysics [Internet]. 2019;92(1):80–8. Available from: https://doi.org/10.1007/s10891-019-01909-7
17. Andrushchak N, Karbovnyk I. LabVIEW-Based Automated Setup for Interferometric Refractive Index Probing. SLAS Technology [Internet]. 2020;25(3):286–92. Available from: https://doi.org/10.1177/2472630319891133
18. Abedini Najafabadi H, Ozalp N, Ophoff C, Moens D. An Experimental Study on Temperature Control of a Solar Receiver Under Transient Solar Load. Solar Energy [Internet]. 2019;186(December 2018):52–9. Available from: https://doi.org/10.1016/j.solener.2019.05.002
19. Hnayno M, Chehade A, Klaba H, Polidori G, Maalouf C. Experimental Investigation of a Data-Centre Cooling System Using a New Single-Phase Immersion/Liquid Technique. Case Studies in Thermal Engineering [Internet]. 2023;45(February):102925. Available from: https://doi.org/10.1016/j.csite.2023.102925
20. Juarsa M, Witoko JP, Giarno, Haryanto D, Purba JH. An Experimental Analysis on Nusselt Number of Natural Circulation Flow in Transient Condition Based on The Height Differences Between Heater and Cooler.

Atom Indonesia [Internet]. 2018;44(3):123–30. Available from: https://aij.batan.go.id/index.php/aij/article/view/876

21. Sørensen SS, Bødker MS, Johra H, Youngman RE, Logunov SL, Bockowski M, et al. Thermal Conductivity of Densified Borosilicate Glasses. Journal of Non-Crystalline Solids. 2021;557(October 2020).
22. Konar D, Sultan MA, Roy S. Numerical Analysis of 2-D Laminar Natural convection heat transfer from Solid horizontal cylinders with Longitudinal Fins. International Journal of Thermal Sciences [Internet]. 2020;154(July 2018):106391. Available from: https://doi.org/10.1016/j.ijthermalsci.2020.106391
23. Morgan VT. The Overall Convective Heat Transfer from Smooth Circular Cylinders. Advances in Heat Transfer [Internet]. 1975;11(C):199–264. Available from: https://doi.org/10.1016/S0065-2717(08)70075-3
24. Bhowmik H, Gharibi A, Yaarubi A, Alawi N. Transient Natural Convection Heat Transfer Analyses From a Horizontal Cylinder. Case Studies in Thermal Engineering [Internet]. 2019;14(September 2018):100422. Available from: https://doi.org/10.1016/j.csite.2019.100422